

Terahertz and infrared photodetectors based on multiple graphene layer and nanoribbon structures

INVITED PAPER

V. RYZHII^{*1,2}, N. RYABOVA^{1,2}, M. RYZHII¹, N.V. BARYSHNIKOV², V.E. KARASIK²,
V. MITIN³, and T. OTSUJI⁴

¹Computational Nanoelectronics Laboratory, University of Aizu, Ikki-machi,
965-8580 Aizu-Wakamatsu, Japan

²Centre for Photonics and Infrared Engineering, Bauman Moscow State Technical University,
5 Vtoraya Baumanskaya Str., 105-005 Moscow, Russia

³Department of Electrical Engineering, University at Buffalo, Buffalo, NY 1460-1920, U.S.A.

⁴Research Institute for Electrical Communication, Tohoku University, Komada, 980-8577 Sendai, Japan

We consider new concepts of terahertz and infrared photodetectors based on multiple graphene layer and multiple graphene nanoribbon structures and we evaluate their responsivity and detectivity. The performance of the detectors under consideration is compared with that of photodetectors made of the traditional structures. We show that due to high values of the quantum efficiency and relatively low rates of thermogeneration, the graphene-based detectors can exhibit high responsivity and detectivity at elevated temperatures in a wide radiation spectrum and can substantially surpass other detectors. The detector being discussed can be used in different wide-band and multi-colour terahertz and infrared systems.

Keywords: terahertz, infrared, photodiode, graphene, nanoribbon.

1. Introduction

Among 3-, 2-, 1-, and 0-dimensional (3D, 2D, 1D, and 0D) carbon structures, whose variety is shown schematically in Fig. 1, graphene layers (GLs), i.e., monolayers of carbon atoms forming a dense honeycomb two-dimensional crystal structure, as well as non-Bernal stacked multiple graphene layers (MGLs) have attracted a considerable attention due to their unique features. In particular, GLs and MGLs exhibit very specific optical properties associated with the gapless energy spectrum and linear dispersion law for electrons and holes (see, for instance, an extensive review by Castro Neto *et al.* [1]). Owing to a rather high quantum efficiency of interband transitions in a single GL (SGL), graphene nanoribbons (GNRs), and graphene bilayers (GBLs) [1,2], they are very promising for detectors of terahertz (THz) and infrared radiation (IR) [3–8]. Indeed, the probability of absorption β , of a photon incident on a GL (at the zero temperature) is expressed via the fundamental constants: $\beta = \pi e^2 / \hbar c = \pi \alpha \cong 0.023$, where e is the electron charge, \hbar is the reduced Planck constant, c is the speed of light in vacuum, and $\alpha = e^2 / \hbar c \cong 1/137$. The quantity β exceeds the probability of the intersubband (intraband) photon absorption in quantum wells by more than the order of magnitude.

Moreover, as demonstrated recently (see the paper by Sprinkle *et al.* [9] as well as the review paper by Orlita and Potemski [10] and the references therein), the stacks of disoriented the non-Bernal stacked GLs epitaxially grown on a C-terminated surface of 4H-SiC, exhibit virtually the same optical spectral characteristics as individual GLs, but much stronger interband absorption. This is because, in contrast to the MGL structures with the Bernal stacking (which normally constitute graphite), the rotational stacking results in the electron decoupling of GLs in the non-Bernal stacked MGLs. As a result, each GL in such a structure exhibits the energy spectrum of electrons and holes similar to that in individual GLs, i.e., the gapless spectrum [10]. Due to the contributions of each GL to the optical absorption, MGLs can exhibit fairly high absorption coefficient. Such a system of MGLs can be considered as a new form of carbon, which constitutes a novel material (which, for brevity, could be referred to as grapheneplex, Ref. 8) for optoelectronics. One of the remarkable feature of this material is high quality of GLs which characterized by fairly long electron and hole momentum relaxation time. The latter provides relatively low intraband (Drude) absorption of radiation.

The use of the MGL structures in question opens up the prospect of farther enhancement of capabilities of graphene-based optoelectronic devices, in particular, THz and IR photodiodes. The GNR structures also exhibit the properties which are very useful for THz and IR detectors. The res-

* e-mail: v-ryzhii@u-aizu.ac.jp

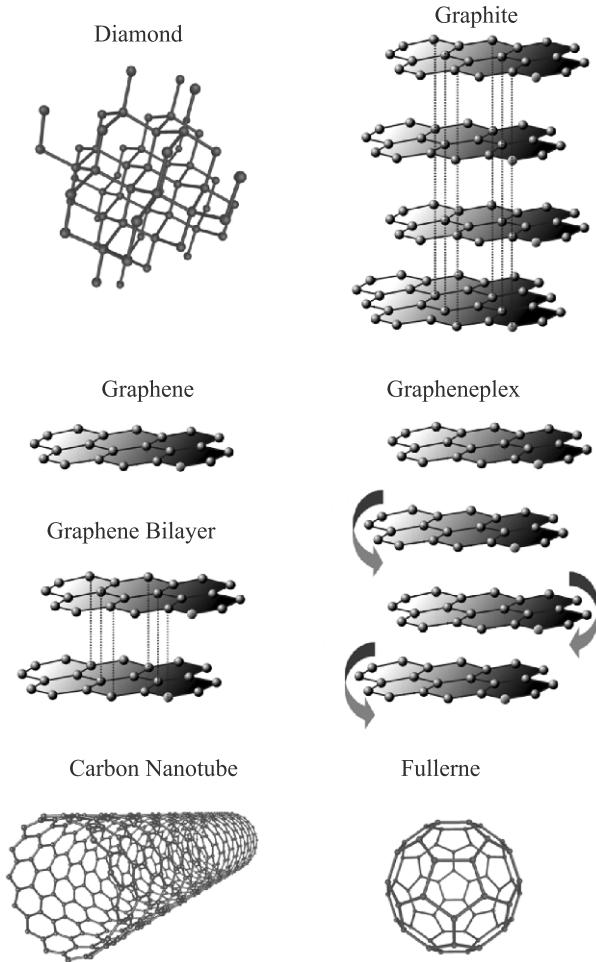


Fig. 1. Schematic view of carbon structures: 3D diamond and graphite; 2D – graphene, graphene bilayer, and multiple graphene structure with disoriented layers (grapheneplex); 1D – carbonnanotube; 0D – fullerene (C₆₀). Arrows at graphene-plex structure indicate disorientation (twist) of non-Bernal stacked graphene layers.

toration of the energy gap in the GNR arrays, which is due to patterning of GL into GNRs, i.e., the formation of an array of quantum wires with the one-dimensional energy subbands, affects the density of states in the conduction and valence bands and, hence, the absorption spectrum and the photodetector spectral characteristics. The emerging of the energy gap promotes a substantial weakening of the interband tunnelling and, consequently, lowering of the dark current and enhancement of the detector detectivity. By virtue of the energy gap in GNR structures, they can be used not only for photodiodes but also for phototransistors [3].

In this paper, we consider the concepts of THz/FIR photodetectors utilizing MGL and GNR structures: the MGL p-i-n photodiode proposed recently [6–8] and the GNR p-i-n photodiode newly proposed in this paper. We develop the device models for MGL and GNR photodiodes and compare their characteristics. We also briefly discuss the MGL and GNR photodiodes potential with that of GNR-phototransistors [3] and GBL phototransistor [4,7] and more traditional photon detectors, particularly, quantum-

-well- and quantum-dot-intersubband photodetectors (QWIPs and QDIPs) as well as interband narrow-gap detectors [11,12]. As shown, the MGL and GNR photodiodes under consideration can surpass the latter photodetectors in responsivity and detectivity, especially, at elevated temperatures. The MGL and GNR p-i-n photodiodes can essentially supplement a wide variety of existing THz and IR detectors [13–17].

2. Device structures and operation principles

Figures 2(a)–2(d) show the structures of MGL and GNR p-i-n photodiodes. In these devices, the MGL and GNR structures are supplied by the side ohmic contacts (source and drain) between which the bias voltage V is applied [see Fig. 3(a)]. The number K , of GLs in the MGL photodiodes can vary from one to dozens [10]. The formation of the p- and n-regions in both MGL and GNR photodiodes can be associated either with the chemical doping as shown in Figs. 2(a) and 2(c) [18] or using the special gates (separated by the gate layer of the thickness W_g) to which the dc voltages $V_p < 0$ and $V_n > 0$ are applied as shown in Fig. 3(a). In the latter case, the side sections of GLs and GNRs are occupied by electrons and holes induced by the transverse electric fields associated with the applied gate voltages [19–21]. The potential profiles in the device with electrically-induced p-i-n junctions in GLs, which are located at different depths from the MGL structure top, are shown in Fig. 3(b). The heights of the barriers μ_k (where $k=1, \dots, K$ is the GL index) at the p-i and i-n junctions are different because the screening of the transverse electric field results in different electron and hole densities and their Fermi energies beneath the gates [21]. In the MGL photodiodes with the chemically doped p- and n-regions, these regions can create the barriers with equal height. As it can be seen in Fig. 3(c), the bias source-drain voltage drops primarily across the i-region (only the potential profile in the top-most GL is shown). This leads to the built-in electric field in the i-region. The operation of the MGL p-i-n-photodiodes is akin to that of the customary p-i-n photodiodes: the electrons and holes, generated by the incident radiation with the photon energy $\hbar\Omega$, are driven to the n- and p-regions, respectively, by the built-in electric field. The motion of the photogenerated electron and hole creates the signal current induced in the external circuit. Due to the gapless energy spectrum of MGLs, the photogeneration in the i-region occurs even at rather low energies of incident photons $\hbar\Omega$.

The structure of GNR p-i-n photodiode is similar to that of SGL p-i-n photodiode. The main distinction is that the uniform GL is replaced (partitioned) by an array of GNRs [see Figs. 2(c) and 2(d)].

In the absence of the electric field in GLs, the spectral dependence of their interband absorption coefficient is given by [2,22]

$$\beta_{\Omega} = \beta[1 - sF(\hbar\Omega/2)] = \beta \tanh\left(\frac{\hbar\Omega}{4k_B T}\right), \quad (1)$$

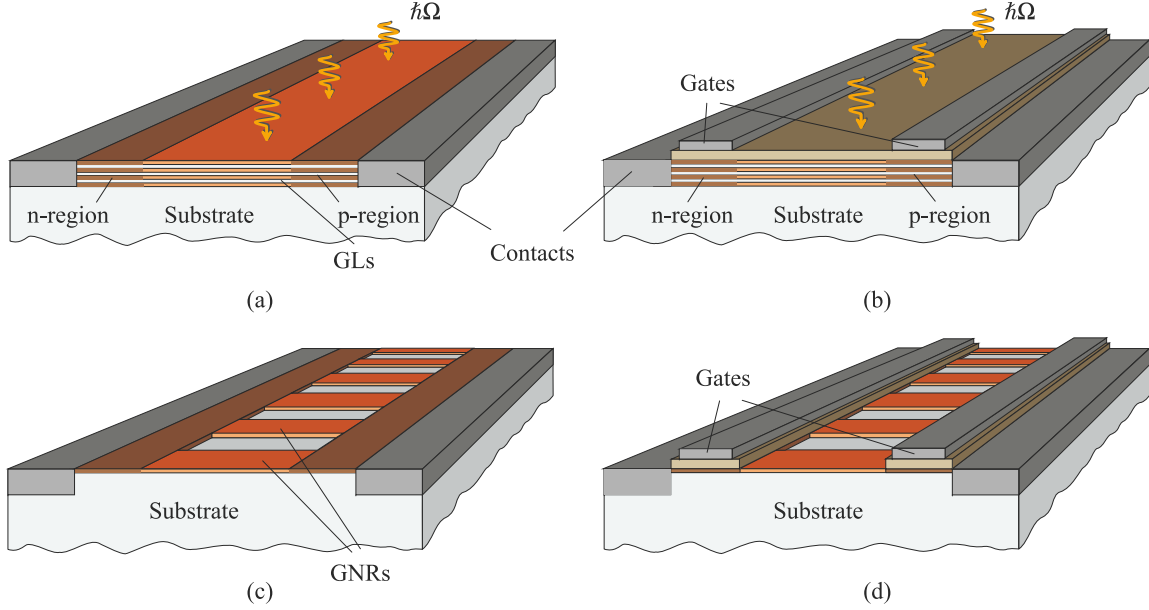


Fig. 2. Schematic views of MGL p-i-n photodiodes with (a) chemically doped p- and n-regions and (b) electrically induced p- and n-regions (electrical doping), as well as of GNR p-i-n photodiodes with (c) chemically doped p- and n-regions and (d) electrically induced p- and n-regions, respectively. A circuit example (for an MGL photodetector with electrically induced p- and n-regions) is shown in Fig. 3(a).

where $\beta \cong 0.023$, $\hbar\Omega$ is the photon energy, $F(\varepsilon) = [\exp(\varepsilon/k_B T) + 1]^{-1}$ is the Fermi distribution function of electrons and holes in equilibrium, T is the temperature, and k_B is the Boltzmann constant. At sufficiently large photon energies $\hbar\Omega > k_B T$, from Eq. (1) we obtain

$$\beta_\Omega \cong \beta = const.. \quad (2)$$

Under the operation conditions, the built-in electric field sweeps out the thermogenerated and photogenerated electrons and holes from the i-region, so that $F(\varepsilon)$ is not the equilibrium Fermi distribution function any more with $F(\varepsilon) \ll 1$ at practically all energies ε . Hence, the term $2F(\hbar\Omega/2)$ in Eq. (1) can be neglected. This validates Eq. (2) for arbitrary photon energies.

The energy spectrum in GNRs is approximately given by

$$\varepsilon_n^\pm = \pm v_W \sqrt{p^2 + (\pi\hbar/d)^2 n^2}, \quad (3)$$

where $v_W = 10^8$ cm/s is the characteristic velocity of electrons and holes in GLs, d is the GNR width, and $n=1, 2, 3, \dots$ is the index of the subband in the valence band (lower sign) and the conduction band (upper sign). According to Eq. (3), the energy gap in GNRs between the subbands in the valence and conduction bands is equal to $\Delta_n = n\Delta = 2\pi v_W \hbar n/d$ (Refs. 3 and 23, i.e., it is proportional to n/d).

The difference in the electron transport and optical properties of GLs and GNR arrays is due to different dimensionality of the electron and hole systems in them: two-dimensional electron and hole systems in GLs and one-dimensional ones in the subbands in the valence and conduction bands of GNRs.

Calculating the interband absorption coefficient of GNRs, one needs to account for the peculiarities of the density of states at the edges of the subbands. To avoid the pertinent divergencies, we introduce a phenomenological parameter Γ ($\Gamma \ll \Delta$), which characterizes the smearing of the subband peculiarities due to the inter-action of electrons and holes with disorder. Owing to this, one can replace the function $\delta(\varepsilon_n^- - \varepsilon_n^+ - \hbar\Omega)$, which reflects the energy conservation for the vertical optical interband transitions between the states with the energies ε_n^- and ε_n^+ in the valence and conduction bands, respectively, by the function $\Gamma/\pi [(\varepsilon_n^- - \varepsilon_n^+ - \hbar\Omega)^2 + \Gamma^2]$ or by $\exp[-(\varepsilon_n^- - \varepsilon_n^+ - \hbar\Omega)^2 / (\sqrt{2\pi}\Gamma)]$ [24].

The value of Γ is about \hbar/τ , where τ is the carrier $2F(1/2)$. momentum relaxation time. In this case, considering the features of the energy spectra or electrons and holes, for the linearly polarized radiation, the spectral dependence of the absorption coefficient in the GNR array can be presented as

$$\beta_\Omega = \beta \cos^2 \psi \left(\frac{2d}{\pi D} \right) \left(\frac{\Delta}{\hbar\Omega} \right) \sum_{n=1}^{\infty} \mathcal{F}_n \left(\frac{\hbar\Omega}{\Delta}, \frac{\Gamma}{\Delta} \right). \quad (4)$$

Here, assuming the Lorentzian or Gaussian energy states broadening, one obtains, respectively

$$\mathcal{F}_n(x, \gamma) = \frac{1}{\pi} \int_n^\infty \frac{d\xi \xi}{\sqrt{\xi^2 - n^2}} \frac{\gamma}{[(\xi - x)^2 + \gamma^2]}, \quad (5)$$

or

$$\mathcal{F}_n(x, \gamma) = \frac{1}{\sqrt{2\pi}\gamma} \int_n^\infty \frac{d\xi \xi}{\sqrt{\xi^2 - n^2}} \exp \left[-\frac{(\xi - x)^2}{2\gamma^2} \right]. \quad (6)$$

Here D is the period of the GNR array in the direction perpendicular to the GNR direction ($d < D$), ψ is the angle between the ac electric field in the incoming THz/IR radiation and the direction of GNRs. The presence of the factor d/D in Eq. (4) reflects the fact that the GNR array covers only a fraction of the irradiated area. When Γ tends to zero, as follows from Eqs. (5) and (6), one obtains $\mathcal{F}_n(x,0) = 1/\sqrt{x^2 - n^2}$, so that Eq. (4) yields (see Ref. 3)

$$\beta_\Omega = \beta \cos^2 \psi \left(\frac{2d}{\pi D} \right) \sum_{n=1}^{\infty} \frac{\Delta \Theta(\hbar\Omega - n\Delta)}{\sqrt{\hbar^2 \Omega^2 - n^2 \Delta^2}}, \quad (7)$$

where $\Theta(\hbar\Omega - n\Delta)$ is the unity step function. The latter dependence on the photon energy differs from that obtained for an array of nanowires with the parabolic dispersion relations for electrons and holes. Indeed, according to Eq. (7), $\beta_\Omega \propto \sum_n \Delta(\hbar^2 \Omega^2 - n^2 \Delta^2)^{-1/2}$ while for the parabolic energy spectrum, one obtains $\beta_\Omega \propto \sum_n \Delta(\hbar\Omega - n\Delta)^{-1/2}$.

If Δ tends to zero (due to an increase in the GNR width d), the summation in the latter equation can be replaced by the integration over dn . After the integration, one can find that

$$\beta_\Omega \equiv \beta \cos \psi \left(\frac{2d}{\pi D} \right) \int_0^{\hbar\Omega/\Delta} \frac{dn}{\sqrt{(\hbar\Omega/\Delta)^2 - n^2}} \equiv \beta \cos \psi \left(\frac{d}{D} \right)$$

Hence, at $d = D$ and $\psi = 0$, one obtains $\beta_\Omega = \beta$.

In Eqs. (4)–(7), we have disregarded the factors associated with the Pauli blocking [as in Eq. (2)] due depletion of the i-region under the dc bias.

As follows from Eqs. (4)–(7), the absorption coefficient exhibits maxima for the resonant transitions between the edges of the subbands in the valence and conduction bands, corresponding to $\hbar\Omega = n\Delta$. In particular, at $\hbar\Omega = \Delta$, the maximum value of β . can be estimated as

$$\max \beta_\Omega \sim \beta \cos^2 \psi \left(\frac{2d}{\pi D} \right) \sqrt{\frac{\Delta}{2\Gamma}}. \quad (8)$$

Equations (4)–(7) are formally valid only when $\beta_\Omega < 1$, i.e., when $\Gamma > \beta^2 \Delta$. The latter inequality is satisfied in any practical conditions.

3. Responsivity of MGL photodiodes

Considering Eq. (2), the current (per unit width perpendicular to its direction) created in a MGL photodiode with K GLs by photogenerated electrons and holes, i.e., the photocurrent, is given by the following formula [6–8]

$$J_{MGL}^{photo} = \frac{4leg[1 - (1 - \beta)^K]}{\hbar\Omega} I. \quad (9)$$

Here, $2l$ is the length of the i-region [see Fig. 3(a)], and I is the power density of incident radiation. The factor g is the photoelectric gain. If the i-region is sufficiently short, so that the electron and hole transit time across this section is

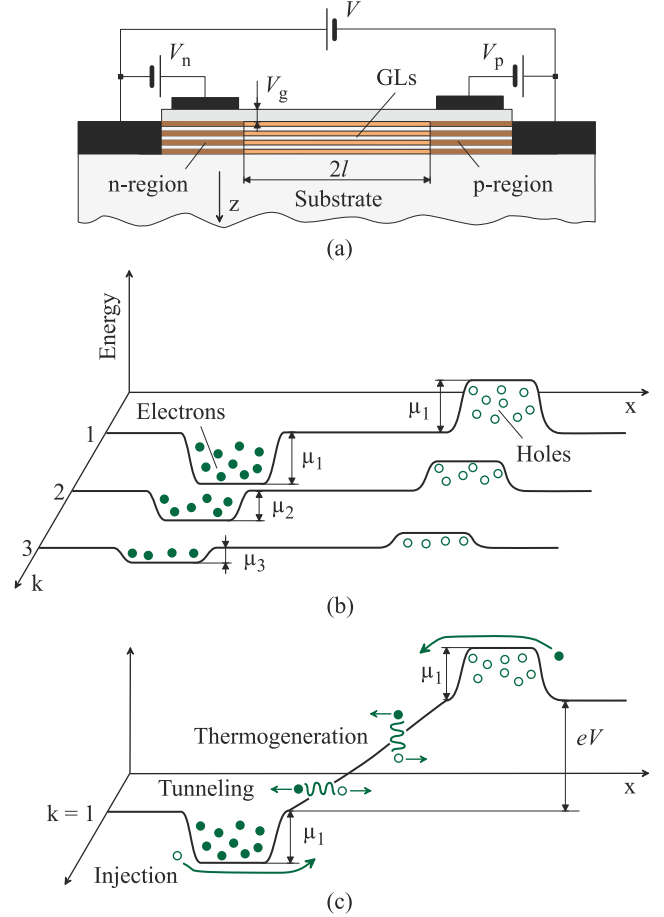


Fig. 3. (a) Structure of MGL photodiode with electrically induced p- and n-regions and the pertinent wiring, (b) energy band diagrams of GLs located at different distances from the top at $V = 0$, and (c) energy band diagram of the top-most GL at reverse bias. Opaque and open circles correspond to electrons and holes accumulated beneath the positively and negatively biased gates, respectively. Arrows show their intraband and interband transitions at dark conditions.

shorter than the characteristic recombination time τ_r , all the photogenerated electrons and holes are managed to contribute to the photocurrent during their propagation across the i-section. In this case, $g \equiv 1$. In the MGL photodiodes with relatively long i-sections, the recombination of the photogenerated electrons and holes decreases their contribution to the photocurrent, so that $g < 1$. Equation (9) accounts for the absorption of THz/IR photons in all GLs and the dependence of the photogeneration rate on the GL index (due to the attenuation of radiation associated with its absorption in the GLs located closer to the structure top). Equation (9) can also be presented as

$$J_{MGL}^{photo} = \frac{4leg\beta K^*}{\hbar\Omega} I, \quad (10)$$

where $K^* = [1 - (1 - \beta)^K] / \beta < K$ can be called the effective number of GLs.

Using Eqs. (9) and (10), the MGL photodiode responsivity, defined as

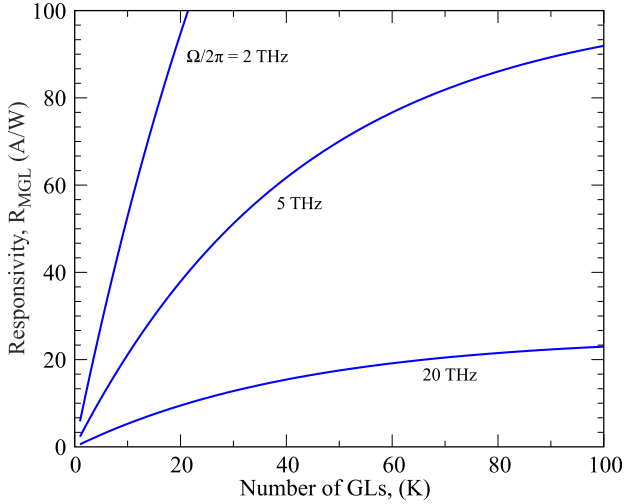


Fig. 4. Responsivity of MGL photodiode as functions of number of GLs for different photon frequencies.

$$R_{MGL} = J_{MGL}^{photo} / 2I, \quad (11)$$

can be presented in the following form

$$R_{MGL} = \frac{4eg[1 - (1 - \beta)^K]}{\hbar\Omega} = \frac{2eg\beta K^*}{\hbar\Omega}. \quad (12)$$

Figure 4 shows the dependence of the responsivity at different photon frequencies $\Omega/2\pi$ calculated for MGL photodiodes with different number of GLs K . Figure 5 shows the responsivity spectral dependences for such photodiodes with $K = 50$ ($K^* \cong 30$) and $K = 10$ ($K^* \cong 9$) as well as that for a SGL ($K = 1$).

4. Responsivity of GNR photodiodes

Accounting for Eq. (4), the photocurrent in the GNR photodiode is given by

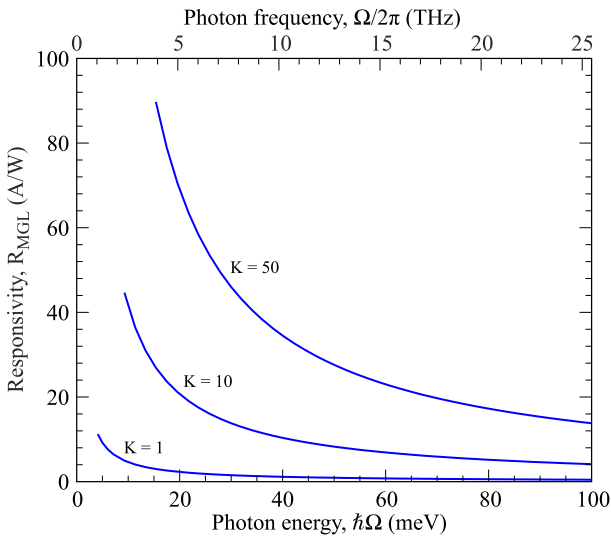


Fig. 5. Responsivity of MGL photodiodes with different number of GLs as a function of the photon energy and frequency.

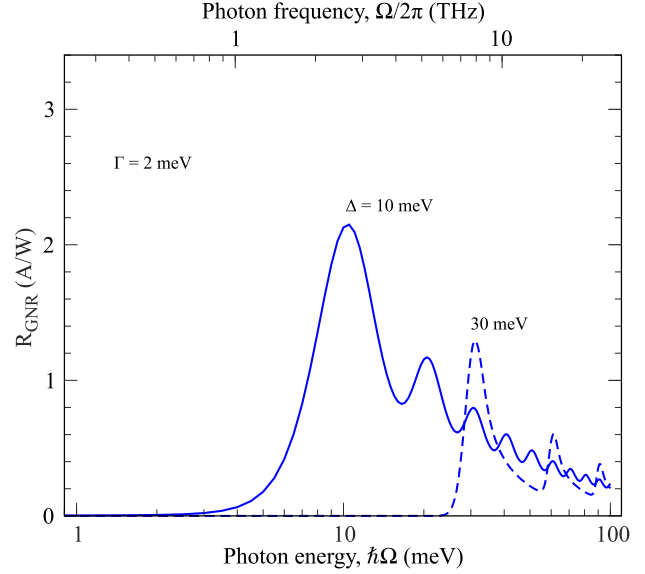


Fig. 6. Responsivity of GNR photodiodes with different values of the energy gap ($\Delta = 10$ meV – solid curve and $\Delta = 30$ meV – dashed curve) as a function of the photon energy and frequency at $\Gamma = 2$ meV.

$$J_{GNR}^{photo} = \frac{8leg\beta \cos^2 \psi d}{\pi D} \left(\frac{I}{\hbar\Omega} \right) \left(\frac{\Delta}{\hbar\Omega} \right) \sum_{n=1}^{\infty} \mathcal{F}_n \left(\frac{\hbar\Omega}{\Delta}, \frac{\Gamma}{\Delta} \right). \quad (13)$$

For the GNR photodiode responsivity, defined by a formula similar to Eq. (11), Eq. (13) yields the following expression

$$R_{GNR} = \frac{2eg\beta \cos^2 \psi}{\hbar\Omega} \left(\frac{2d}{\pi D} \right) \left(\frac{\Delta}{\hbar\Omega} \right) \sum_{n=1}^{\infty} \mathcal{F}_n \left(\frac{\hbar\Omega}{\Delta}, \frac{\Gamma}{\Delta} \right). \quad (14)$$

At $\hbar\Omega = \Delta$ and $\psi = 0$, the GNR photodiode responsivity reaches a maximum

$$\max R_{GNR} \cong \frac{eg\beta}{\sqrt{\Gamma\Delta}} \left(\frac{d}{D} \right). \quad (15)$$

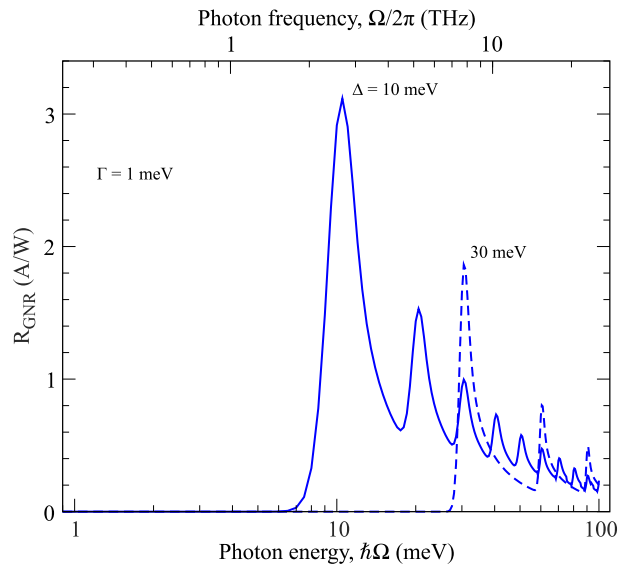


Fig. 7. The same as in Fig. 6 but at $\Gamma = 1$ meV.

The spectral dependences of the responsivity of GNR photodiodes with different values of the energy gap Δ calculated using Eqs. (6) and (14) are demonstrated in Figs. 6 and 7. It is assumed that $\psi = 0$, $d = D/2$, and $\Gamma = 2$ and 1 meV. The latter corresponds to $\tau \cong (3-6) \times 10^{-13}$ s.

Using Eqs. (11) and (15), for the ration of the responsivities of a MGL photodiode and the maximum responsivity of a GNR photodiode (at $\hbar\Omega = \Delta$) one can find

$$\frac{\max R_{GNR}}{R_{MGL}} \cong \sqrt{\frac{\Delta}{\Gamma}} \left(\frac{d}{D} \right) \frac{1}{K^*}. \quad (16)$$

The first factor in Eq. (16) can be large in GNR photodiodes with sufficiently perfect GNRs, while the other two can be of the order of unity or small. The latter occurs if the GNR density is small ($d \ll D$) and/or the MGL photodetector under consideration includes many GLs ($K > K^* \gg 1$). Thus, the responsivity of MGL photodiodes with rather large number of GL is markedly larger than the maximum responsivity of GNR photodiodes. However, SGL and GNR photodiodes exhibit similar responsivities. This is because the quantum efficiency in MGL photodiodes can be rather large (approaching to two if $K \gg 1$), while the smearing of the subband edges due to disorder pronouncedly limits the resonant enhancement of the interband absorption coefficient in GNRs and, consequently, the quantum efficiency in GNR photodiodes.

Indeed, Eqs. (11) and (14) can be presented as

$$R_{MGL} = \frac{eg}{\hbar\Omega} \eta_{MGL}, \quad R_{GNR} = \frac{eg}{\hbar\Omega} \eta_{GNR}, \quad (17)$$

where

$$\eta_{MGL} = 2\beta K^*, \quad (18)$$

(in a wide range of the photon energies) and

$$\eta_{GNR} \cong \beta \cos^2 \psi \left(\frac{d}{D} \right) \sqrt{\frac{\Delta}{\Gamma}}, \quad (19)$$

(at $\hbar\Omega = \Delta$) are the quantum efficiencies of MGL and GNR structures, respectively. For $K = 1-50$, Eq. (11) yields $\eta_{MGL} \cong 0.046-1.38$. One needs to stress that the quantity η_{MGL} can exceed unity (but it is smaller than two) because the interband absorption of a photon leads to the generation both an electron and a hole. Simultaneously, for the parameters used in the above estimate, we find $\eta_{GNR} \cong 0.023-0.07$.

The responsivities of both MGL and GNR photodiodes decreases with increasing photon energy. As for MGL photodiodes, $R_{MGL} \propto 1/\hbar\Omega$. Such dependence is attributed to the quantum efficiency independent of $\hbar\Omega$. and to the decreasing number of incident photons with increasing their energy and fixed intensity. The pertinent dependence in GNR photodiodes is complicated by an additional resonant factor.

5. Dark-current limited detectivity of MGL photodiodes

The dark-current limited detectivity D^* is usually defined as $D^* = (J^{photo}/NP) \cdot \sqrt{A\Delta f}$, where $P = AI$ is the power rece-

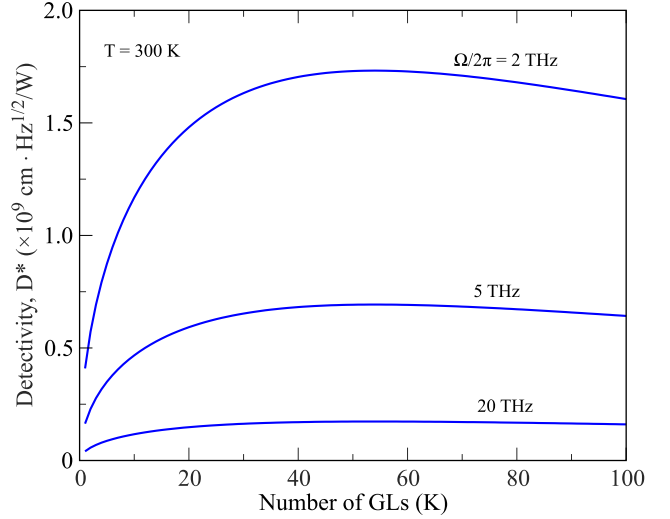


Fig. 8. Thermogeneration limited detectivity of MGL p-i-n photodiodes at different photon frequencies as functions of number of GLs.

ived by the photodetector, $A = 2lH$ and H are the device area and width in the direction perpendicular to the current, Δf is the bandwidth, and N is the noise [25]. The noise can be expressed via the dark current J^{dark} , as $N = (4eg^{noise} J^{dark} H\Delta f)^{1/2}$, where g^{noise} is the noise gain. Hence, the dark-current limited detectivity of MGL and GNR photodiodes can be presented respectively as

$$D_{MGL}^* = R_{MGL} \sqrt{\frac{A}{4eJ_{MGL}^{dark} H}}, \quad (20)$$

$$D_{GNR}^* = R_{GNR} \sqrt{\frac{A}{4eJ_{GNR}^{dark} H}}. \quad (21)$$

The dark current, which comprises the component associated with the interband thermogeneration and tunnelling generation of electrons and holes in the i-section

$$J_{GML}^{dark} = 4KeI(G^{th} + G^{tunn}) + 2KJ^{inj}, \quad (22)$$

where G^{th} and G^{tunn} are the thermogeneration and tunnelling rates in each GL per unit of its area and J^{inj} is the current of electrons injected from the p-region and the current of holes injected from the n-region (minority carrier currents).

Expressing the noise via the dark current, using Eqs. (18), and setting $g = g^{noise} = 1$, we obtain

$$D_{MGL}^* = \frac{K^* \beta}{\hbar\Omega \sqrt{2K(G^{th} + G^{tunn} + J^{inj}/2eI)}}. \quad (23)$$

At not too low temperatures, the interband thermogeneration is primarily associated with the absorption of optical phonons [26]. Considering that the number of optical phonons at the temperature $T \ll \hbar\omega_0/k_B$ is equal to $N' \cong \exp(-\hbar\omega_0/k_B T)$, where $\hbar\omega_0 \cong 0.2$ eV is the optical phonon energy and k_B is the Boltzmann constant, we shall use the following simplified formula

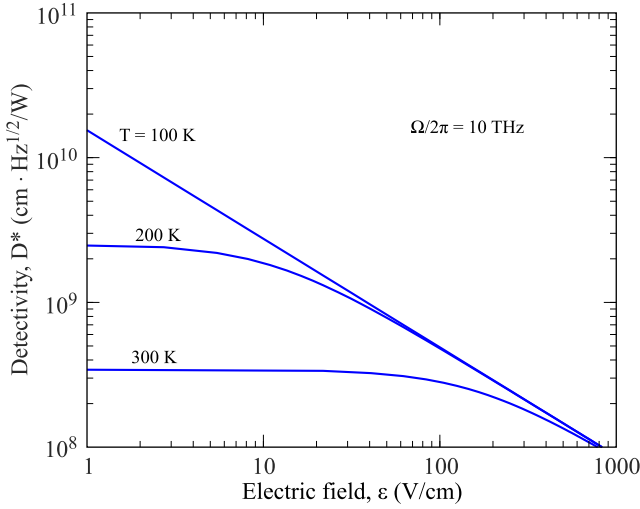


Fig. 9. MGL photodiode detectivity for $\Omega/2\pi = 10$ THz as a function of the electric field at different temperatures.

$$G_{MGL}^{th} = \overline{G}^{th} \exp\left(-\frac{\hbar\omega_0}{k_B T}\right), \quad (24)$$

where \overline{G}^{th} is a pre-exponential factor, which for simplicity is assumed to be independent of the temperature. Comparing Eq. (24) with the results of numerical calculations, we set $\overline{G}^{th} = 3 \times 10^{24} \text{ cm}^{-2}\text{s}^{-1}$, so that at $T = 300$ K one obtains $G^{th} \sim 10^{21} \text{ cm}^{-2}\text{s}^{-1}$ [26].

The interband tunnelling rate in a GL at the electric field $\varepsilon = V/2l$ is given by [19,20,27]

$$G_{MGL}^{tunn} = \frac{1}{4\pi v_W^{1/2}} \left(\frac{eV}{2\hbar}\right)^{3/2} = B^{tunn} \left(\frac{V}{2l}\right)^{3/2}. \quad (25)$$

Here, $v_W = 10^8$ cm/s is the characteristic velocity of electrons and holes in GLs and $B^{tunn} = [(e/\hbar)^{3/2}/4\pi v_W^{1/2}] \approx 5 \times 10^{17} \text{ s}^{-1}\text{cm}^{-1/2}\text{V}^{-3/2}$. The injection current is determined by the height of the barrier μ [see Fig. 2(c)] formed due to doping of the pertinent regions

$$J_{MGL}^{inj} = \overline{J}^{inj} \exp\left(-\frac{\mu}{k_B T}\right), \quad (26)$$

where $\overline{J}^{inj} = 2e(k_B T)^2 / \pi^2 \hbar^2 v_W$.

The quantity μ in the GL p-i-n photodiodes with chemical doping can be expressed in terms of the donor and acceptor density per one GL Σ_i as $\mu \approx \hbar v_W \sqrt{\pi \Sigma_i}$. In the MGL photodiodes with electrically induced p- and n-regions, the barrier heights in different GLs are different ($\mu_1 > \mu_2 > \dots$) due to the screening of the transverse electric field created by the voltages V_n and V_p [see Fig. 2(b)] [21]. Due to this, the net injection current can be rather significant if in GLs with large indices ($k \sim K$) the barrier are insufficiently high. In the case of high doping of the p- and n-regions or at sufficiently high voltages V_p and V_n and not too large num-

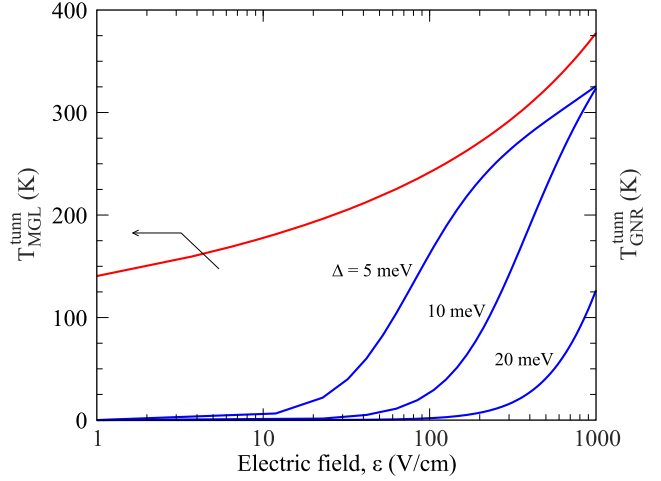


Fig. 10. Electric field dependences of characteristic temperatures T_{MGL}^{tunn} (left scale) and T_{GNR}^{tunn} (right scale) for different energy gaps Δ , corresponding to resonant frequencies $\Omega/2\pi = \Delta/2\pi\hbar = 1.27, 2.54,$ and 5.09 THz, respectively. The areas above and below the pertinent curve correspond to dominating thermogeneration and tunnelling dark current mechanisms, respectively.

ber of GLs, the injection current can be small in comparison with the thermionic and tunnelling currents. The injection current can be disregarded if $2eIG^{th} \exp(-\hbar\omega_0/k_B T) \gg \overline{J}^{inj} \exp(-\mu/k_B T)$, i.e., when $\mu > \hbar\omega_0 + k_B T \ln(\overline{J}^{inj}/2eIG^{th})$. Assuming $2l = 10 \mu\text{m}$ and $T = 300$ K, we obtain $\mu > \approx 71$ meV or $\Sigma_i > 4 \times 10^{11} \text{ cm}^{-2}$. At the larger l , the previous condition becomes even more liberal. However, the dark current associated with the thermogeneration decreases with decreasing temperature faster than the injection current. Consequently, at low temperatures, the injection current as well as the tunnelling current can be the main mechanisms of the dark current limiting the detectivity. The injection dark current can also dominate in GL p-i-n photodiodes with electrically induced p- and n-regions if the number of GLs K is excessively large.

Neglecting the injection current and combining Eqs. (23)–(25), we arrive at [6]

$$D_{MGL}^* = \frac{K^* \beta}{\hbar\Omega \sqrt{2K \left[\overline{G}^{th} \exp\left(-\frac{\hbar\omega_0}{k_B T}\right) + B^{tunn} \left(\frac{V}{2l}\right)^{3/2} \right]}}. \quad (27)$$

As seen from Eq. (27), the detectivity depends on the number of GLs, the temperature, and the electric field in the i-region. At elevated temperatures and not too strong electric fields, the dark current and, consequently, the detectivity are determined mainly the thermogeneration. The dependences of the MGL photodiode detectivity D_{MGL}^* limited by the thermogeneration dark current on the number of GLs K calculated for different radiation frequencies $\Omega/2\pi$ at $T = 300$ K are shown in Fig. 5.

One can see that the responsivity of MGL-photodiodes increases sub-linearly with increasing number of GL. This

is natural because the quantum efficiency η rises when K and, consequently, K^* increase. As follows from Fig. 5, at the sufficiently large number of GLs, the responsivity is very high. This is attributed to a strong interband absorption (in each of the multiple GLs) and almost flat its spectral dependence.

As it is seen from Fig. 8, the detectivity as a function of number of GLs reaches a maximum and then slightly decreases. This is because K^* , as a function of K , saturates at large K , while the contribution of the dark current to the detectivity is proportional to $1/\sqrt{K}$. As a result, the detectivity reaches a maximum at K about few dozens. Indeed, the function $K^*\beta/\sqrt{K} = [1 - (1 - \beta)^K] / \sqrt{K} \cong [1 - \exp(-\beta K)] / \sqrt{K}$ and, hence, D^* reaches maxima at $K = K_{max} = 55$ with $K^*\beta/\sqrt{K} \cong 0.097$.

Figure 9 shows the detectivity of a MGL photodiode with $K = 50$ and $K^* \cong 30$ as a function of the electric field in the i-region $\varepsilon = V/2l$ calculated for different temperatures. One can see from Fig. 9, that at relatively low temperatures, an increase in the electric field can lead to a dramatic fall in the detectivity. The latter is due to a significant increase in the tunnelling current at elevated electric fields, particularly at low temperatures. At higher temperatures, this effect is much less pronounced because the dark current is primarily limited by the thermogeneration (compare the electric field dependences in Fig. 9 for $T = 100, 200,$ and 300 K. Moreover, as seen, the detectivity is virtually independent on ε in the interval $\varepsilon = 1 - 10$ V/cm in the temperature range $T = 200 - 300$ K.

One can introduce the characteristic temperature T_{MGL}^{tunn} , at which the thermogeneration rate given by Eq. (24) is equal to the tunnelling rate given by Eq. (25). Equations (24) and (25) result in the following equation which relates T_{MGL}^{tunn} and the electric field $\varepsilon = V/2l$

$$T_{MGL}^{tunn} = \frac{\hbar\omega_0}{k_B \ln(\varepsilon_{MGL}^{tunn}/\varepsilon)^{3/2}}, \quad (28)$$

where $\varepsilon_{MGL}^{tunn} = (\overline{G^{th}}/\overline{B^{tunn}})^{2/3}$. Thus, at $T > T_{MGL}^{tunn}$, the MGL photodiode detectivity is primarily limited by the thermogeneration, while at $T < T_{MGL}^{tunn}$ it is limited by the tunnelling. Estimating ε_{MGL}^{tunn} , one can obtain $\varepsilon_{MGL}^{tunn} \cong 6 \times 10^4$ V/cm.

6. Dark current limited detectivity of GNR photodiodes

The energy gap Δ , in the GNRs under consideration is smaller than the optical phonon energy $\hbar\omega_0$. Due to this, the thermogeneration rate in MGL and GNR photodiodes is of the same order of magnitude. This implies that the detectivities of these photodiodes at elevated temperatures, say, at $T = 300$ K (when the thermogeneration provides the main contribution to the dark current), and $\hbar\Omega \geq \Delta$ are close

to each other. However, at relatively low temperatures, at which the interband tunnelling becomes more effective than the thermogeneration, GNR photodiodes can surpass GBL photodiodes in detectivity. This is possible due to the energy gap which suppresses the interband tunnelling and, hence, the dark current.

The current associated with the interband tunnelling in the i-region can be estimated considering that the tunnelling probability between the lowest subband in the conduction band and the top-most subband in the valence band is given by [19,20]

$$P_{tunn} = \exp\left[-\frac{\pi^3 \hbar v_W}{d^2} \left(\frac{2l}{eV}\right)\right]. \quad (29)$$

Considering this, the rate of interband tunnelling generation rate in the i-section can be estimated can be presented in the following form

$$\begin{aligned} G_{GNR}^{tunn} &\cong \frac{eV}{8Dl\hbar} \exp\left[-\frac{\pi^3 \hbar v_W}{d^2} \left(\frac{2l}{eV}\right)\right] \\ &= \frac{eV}{8Dl\hbar} \exp\left[-\frac{\pi\Delta^2}{4\hbar v_W} \left(\frac{2l}{eV}\right)\right]. \end{aligned} \quad (30)$$

Comparing Eqs. (25) and (30), one can find that

$$\begin{aligned} G_{GNR}^{tunn} &\cong G_{MGL}^{tunn} \sqrt{\frac{4\pi^2 \hbar v_W}{D^2} \left(\frac{2l}{eV}\right)} \exp\left[-\frac{\pi^3 \hbar v_W}{d^2} \left(\frac{2l}{eV}\right)\right] \\ &= G_{MGL}^{tunn} \sqrt{\frac{4\pi^2 \hbar v_W}{D^2} \left(\frac{2l}{eV}\right)} \exp\left[-\frac{\pi\Delta^2}{4\hbar v_W} \left(\frac{2l}{eV}\right)\right]. \end{aligned} \quad (31)$$

Using Eqs. (21) and (31), we arrive at the following formula for the dark-current (tunnelling) limited GNR photodiode detectivity

$$\frac{D_{GNR}^*}{D_{MGL}^*} \cong \frac{R_{GNR}}{R_{MGL}} \left(\frac{D^2 e\varepsilon}{4\pi^2 \hbar v_W}\right)^{1/4} \exp\left(\frac{\pi\Delta^2}{8\hbar v_W e\varepsilon}\right). \quad (32)$$

At $\hbar\Omega = \Delta$, fixing the ratio $d/D = 1/2$ and using the relationship between d and Δ , from Eqs. (16) and (29) we obtain (disregarding a numerical factor of the order of unity) the following rather transparent formula

$$\frac{\max D_{GNR}^*}{D_{MGL}^*} \cong \sqrt{\frac{\Delta}{\Gamma}} \frac{\exp(\varepsilon_{GNR}^{tunn}/\varepsilon)}{(\varepsilon_{GNR}^{tunn}/\varepsilon)^{1/4}} \frac{1}{K^*}, \quad (33)$$

where $\varepsilon_{GNR}^{tunn} = (\pi\Delta^2/8e\hbar v_W)$. The quantity ε_{GNR}^{tunn} varies from $2\pi \times 10^2$ V/cm at $\Delta = 10$ meV to $2\pi \times 10^4$ V/cm at $\Delta = 100$ meV. Equation (33) includes the factor $\sqrt{\Delta/\Gamma}$, associated with the resonant character of the interband optical transitions, which can be large when the subband edge smearing Γ is small, as well as a large exponential factor. The latter is associated with the suppression of the interband tunnelling with increasing energy gap Δ . It also includes

a factor the factor $1/K^*$ which is small in MGL photodiodes with a large number of GLs K .

One can also introduce the characteristic temperature T_{GNR}^{tunn} for GNR photodiodes, so that the temperature ranges $T > T_{GNR}^{tunn}$ and $T < T_{GNR}^{tunn}$ correspond to the domination of thermogeneration and tunnelling, respectively. The introduced quantity is governed by the following equation [compare with Eq. (28) in Sect. 5]

$$T_{GNR}^{tunn} = \frac{\hbar\omega_0}{k_B [\ln(\epsilon_{MGL}^{tunn}/\epsilon)]^{3/2} (\epsilon/\epsilon_{MGL}^{tunn})^{1/2} + 2(\epsilon_{MGL}^{tunn}/\epsilon)}. \quad (34)$$

Figure 10 shows the $T_{MGL}^{tunn} - \epsilon$ (and $T_{MGL}^{tunn} - \epsilon$ dependences, calculated using Eqs. (28) and (34), respectively.

Thus, at moderate electric field the interband tunnelling in GNR photodiodes is not a crucial mechanism markedly limiting the detectivity even at rather low temperatures.

7. GNR photodiodes vs. phototransistors

As pointed out in Sect. 3, the photoelectric gain of MGL and GNR photodiodes $g \leq 1$. This is because an absorbed photon generates one electron and one hole, which induce the signal (terminal) current during their propagation across the i -region. The recombination can limit the contribution of the photogenerated electrons and holes to the signal current (leading to a decrease in g) if the characteristic drift length $l_r = \mu\epsilon\tau_r < 2l$. Here, μ is the electron and hole mobility in the i -region of MGL or GNR photodiode.

As follows from Fig. 9, the detectivity of MGL and GBR photodiodes at room temperature as a function of the electric field saturates at $\epsilon \leq 100$ V/cm. Assuming that $\epsilon = 100$ V/cm, $\mu = (1 - 2) \times 10^4$ cm²V⁻¹s⁻¹, and $\tau_r = 10^{-10}$ s, one can obtain the following estimate for the drift length $l_r \cong (1-2)$ μ m. Such a length is markedly smaller than the THz radiation wavelength $\lambda = 2\pi c/\Omega$, that can result in the problems associated with the radiation coupling [15]. Thus, in the case of MGL photodiodes, one needs either to increase the electric field (the bias voltage), sacrificing the detectivity value, or to use special antenna or grating for effective coupling of radiation. At lower temperatures and higher mobility, the situation becomes easier. Indeed, at $T \leq 150$ K, setting $\epsilon = 100$ V/cm, $\mu = (5 - 20) \times 10^4$ cm²V⁻¹s⁻¹, and $\tau_r = 10^{-9}$ s, we obtain $l_r \cong 50-200$ μ m.

Since the interband tunnelling in GNR photodiodes can be effectively suppressed, the electric field in the i -region (bias voltage) can be chosen sufficiently large to provide rather long recombination length. The latter yields the opportunity to use fairly long GNRs.

However, in contrast to the two-terminal devices (GNR photodiodes), in the GNR n-p-n field-effect transistors (GNR p-n-p transistors) with the structure similar to that of GNR photodiodes but with an additional highly conducting electrically floating gate between the side source and drain n-contacts (p-contacts), one can achieve rather high values of the photoelectric gain [3]. Such GNR n-p-n transistors

being actually also two-terminal devices can serve as phototransistors. In such GNR phototransistors, the photogenerated holes (electrons) are accumulated beneath the gate resulting in the lowering of the barrier for the electrons (holes) injected from the source and collected by the drain. Due to relatively long lifetime of holes (electrons) captured under the gate, the photoelectric gain can be fairly large.

As demonstrated previously, the photoelectric gain in GNR phototransistors can be of the order of $eV/k_B T \gg 1$ [3]. The effect of elevated photoelectric gain can be achieved also in THz and IR detectors based on phototransistors GBL structures, in which the gap opening is due to the transverse electric field created by the gate voltage [4]. High photoelectric gain in GNR and GBL phototransistor might provide some their advantages over GNR photodiodes but by utilizing more complex device structures. The presence of the gate over the GNR and GBL phototransistors can, however, result in a marked deterioration of the electron and hole mobility in GNRs and GBL.

8. GBL and GNR photodiodes vs. some other THZ and IR detectors

The detection of THz and far IR radiation can, in principle, be realized using the interband transition in the structures with bulk semiconductors like mercury-cadmium-tellurium (MCT) with sufficiently narrow energy gap [16]. Leaving aside the fabrication problems, let us compare MGL and GNR photodiodes with and MCT photodiodes. The absorption coefficients in both MGL and MCT photodiodes can be close to unity. Hence, both of them can exhibit similar quantum efficiencies. However, the dark current associated with the thermogeneration of electrons and holes, i.e., the factor crucially affecting the detectivity, in GNR photodiodes, should be much lower than in MCT photodiodes. This is because the energy of optical phonons in MGLs $\hbar\omega_0 \cong 0.2$ eV in GLs is much larger than optical phonon energy in MCT. As a result, even at the room temperatures, the number of optical phonons in MGL photodiodes $N_0 \cong \exp(-\hbar\omega_0/k_B T) \ll 1$. Due to this, the thermogeneration associated with the absorption of optical phonons in GLs is relatively weak (it is proportional to exponentially small number N_0). Next mechanism which could contribute to the thermogeneration in GLs is the absorption of acoustic phonons. However, due to small velocity of acoustic waves s in comparison with the characteristic velocity of electrons and holes in GLs $v_w = 10^8$ cm/s, the one-phonon interband absorption is forbidden. The Auger processes, which are fairly strong in MCT, are also forbidden in GLs due to the linear dispersion relation for electrons and holes [28]. Thus, one can expect that MGL and GNR photodiodes can markedly surpass MCT photodiodes in the dark-current limited detectivity.

Further development of QWIPs and QDIPs has also resulted in the possibility of THz and far IR detection in these devices [29]. However, the absorption coefficients in

a QW and a QD array is about one order of magnitude smaller than in a GL (for instance, $\beta_{QW} \sim 0.002$). The photoionization energy of electrons (or holes) in QWs and QDs ε_i should be sufficiently small to provide the condition $\hbar\Omega \geq \varepsilon_i$. Due to a smallness of ε_i , the thermoexcitation rate in QWIPs and QDIPs due to the absorption of optical phonons appears to be much higher than in MGL and GNR photodiodes. Apart from this, the tunnelling from QWs and QDs can also greatly contribute to the dark current limiting the QWIP/QDIP performance.

9. Conclusions

We calculated the responsivity and dark-current limited detectivity of MGL and GNR photodiodes as THz and IR detectors. Using the developed device models, we demonstrated that due to high values of the quantum efficiency MGL and GNR photodiodes can exhibit fairly high responsivity in the THz and IR ranges. It was shown that at room temperatures the thermogeneration of electrons and holes associated with optical phonon absorption is the dominant mechanism limiting the detectivity. However, owing to relatively low probability of the optical phonon absorption in GLs and GNRs associated with rather large phonon energy, the room temperature detectivity can be fairly high. As shown, the interband tunnelling can be an essential mechanism determining the dark current and, hence, the MGL photodiode detectivity at lowered temperatures ($T \leq 250$ K). This mechanism limits the ultimate values of the detectivity and necessitates the optimization of the device structure and proper choice of the temperature and the bias voltage. In contrast, in GNR photodiodes with an open energy gap, the interband tunnelling can be insignificant even at rather strong electric fields (high bias voltages) in the i-region in a wide temperature range. Thus, the detectors under consideration can exhibit high responsivity and detectivity at elevated temperatures, in particular, at room temperatures, in a wide radiation spectrum and can substantially surpass other detectors.

The combination of high responsivity and detectivity with other features of the photodetectors under consideration (spectral and polarization dependences) is considerably promising for their application in different wide-band (based on MGL photodiodes) and multi-colour (based on GNR photodiodes with different width of GNRs) THz and IR systems.

Acknowledgements

The authors are grateful to V.I. Pustovoi, A.M. Philachev, and V.P. Ponomarenko for useful and stimulating discussion. The work at the University of Aizu and Tohoku University was funded by the Japan Science and Technology Agency, CREST, and by the Japan Society for promotion of Science, Japan. The work at the University at Buffalo was supported by the National Science Foundation, TERANO Project, USA.

References

1. A.H. Castro Neto, F. Guinea, N.M.R. Peres, K.S. Novoselov, and A.K. Geim, "The electronic properties of graphene", *Rev. Mod. Phys.* **81**, 109–162 (2009).
2. L.A. Falkovsky and A.A. Varlamov, "Space-time dispersion of graphene conductivity", *Eur. Phys. J.* **B56**, 281–284 (2007).
3. V. Ryzhii, V. Mitin, M. Ryzhii, N. Ryabova, and T. Otsuji, "Device model for graphene nanoribbon phototransistor", *Appl. Phys. Express* **1**, 063002 (2008).
4. V. Ryzhii and M. Ryzhii, "Graphene bilayer field-effect phototransistor for terahertz and infrared detection", *Phys. Rev.* **B79**, 245311 (2009).
5. F. Xia, T. Murler, Y.M. Lin, A. Valdes-Garcia, and F. Avouris, "Ultrafast graphene photodetector", *Nat. Nanotechnol.* **4**, 839–843 (2009).
6. V. Ryzhii, M. Ryzhii, V. Mitin, and T. Otsuji, "Terahertz and infrared photodetection using p-i-n multiple-graphene structures", *J. Appl. Phys.* **106**, 084512 (2009).
7. V. Ryzhii, M. Ryzhii, N. Ryabova, V. Mitin, and T. Otsuji, "Terahertz and infrared detectors based on graphene structures", *J. Infrared Phys. Technol.* **54**, 302–305 (2011).
8. M. Ryzhii, T. Otsuji, V. Mitin, and V. Ryzhii, "Characteristics of p-i-n terahertz and infrared photodiodes based on multiple graphene layer structures", *Jpn. J. Appl. Phys.* **50**, 070117-1-6 (2011).
9. M. Sprinkle, D. Suegel, Y. Hu, J. Hicks, A. Tejada, A. Taleb-Ibrahimi, P. Le Fevre, F. Bertran, S. Vizzini, H. Enriquez, S. Chiang, P. Soukiassian, C. Berger, W.A. de Heer, A. Lanzara, and E.H. Conrad, "First direct observation of a nearly ideal graphene band structure", *Phys. Rev. Lett.* **103**, 226803 (2009).
10. M. Orlita and M. Potemski, "Dirac electronic states in graphene systems: optical spectroscopy studies", *Semicond. Sci. Tech.* **25**, 063001-1-21 (2010).
11. V. Ryzhii, I. Khmyrova, M. Ryzhii, and V. Mitin, "Comparison of dark current, responsivity and detectivity of different intersubband infrared photodetectors", *Semicond. Sci. Tech.* **19**, 8–16 (2004).
12. A. Rogalski, J. Antoszewski, and L. Faraone, "Third generation infrared photodetector arrays", *J. Appl. Phys.* **105**, 091101 (2009).
13. V. Ryzhii, "The theory of the quantum-dot infrared phototransistor", *Semicond. Sci. Tech.* **11**, 759–765 (1996).
14. K.K. Choi, *The Physics of Quantum Well Infrared Photodetectors*, World Scientific, Singapore, 1997.
15. *Intersubband Infrared Photodetectors*, edited by V. Ryzhii, World Scientific, Singapore, 2003.
16. A. Rogalski, J. Antoszewski, and L. Faraone, "Third generation infrared photodetector arrays", *J. Appl. Phys.* **105**, 091101 (2009).
17. A. Rogalski, *Infrared Detectors*, Taylor & Francis, 2010.
18. D. Farmer, Y.M. Lin, A. Afzali-Ardakani, and P. Avouris, "Behaviour of a chemically doped graphene junction", *Appl. Phys. Lett.* **94**, 213106 (2009).
19. V.V. Cheianov and V.I. Fal'ko, "Selective transmission of Dirac electrons and ballistic magneto resistance of n-p junctions in graphene", *Phys. Rev.* **B74**, 041403 (R) (2006).
20. A. Ossipov, M. Titov, and C.W.J. Beenakker, "Re-entrance effect in a graphene n-p-n junction coupled to a superconductor", *Phys. Rev.* **B75**, 251401 (R) (2007).

21. M. Ryzhii, V. Ryzhii, V. Mitin, T. Otsuji, and M.S. Shur, “Electrically induced n-i-p junctions in multiple graphene layer structures”, *Phys. Rev.* **B82**, 075419 (2010).
22. L.A. Falkovsky and S.S. Perhoguba, “Optical far-infrared properties of a graphene monolayer and multilayer”, *Phys. Rev.* **B76**, 153410 (2007).
23. V.V. Popov, T.Yu. Bagaeva, T. Otsuji, and V. Ryzhii, “Oblique terahertz plasmons in graphene nanoribbon arrays”, *Phys. Rev.* **B81**, 073404 (2010).
24. F.T. Vasko and A.V. Kuznetsov, *Electronic States and Optical Transitions in Semiconductor Heterostructures*, Springer, New York, 1998.
25. A. Rose, *Concepts in Photoconductivity and Allied Problems*, Wiley, New York, 1963.
26. F. Rana, P.A. George, J.H. Strait, S. Shivaraman, M. Chanrashekhar, and M.G. Spencer, “Carrier recombination and generation rates for intravalley and intervalley phonon scattering in graphene”, *Phys. Rev.* **B79**, 115447-1-5 (2009).
27. V. Ryzhii, M. Ryzhii, and T. Otsuji, “Thermionic and tunneling transport mechanisms in graphene field-effect transistors”, *Phys. Stat. Sol. (a)* **205**, 1527–1533(2008).
28. M.S. Foster and I.L. Aleiner, “Slow imbalance relaxation and thermoelectric transport in graphene”, *Phys. Rev.* **B79**, 085415 (2009).
29. H. Luo, H.C. Liu, C.Y. Song, and Z.R. Wasilevskim, “Background-limited terahertz quantum-well photodetector”, *Appl. Phys. Lett.* **86**, 231103–231105 (2005).